BBA - Molecular Basis of Disease 1864 (2018) 1183–1191

Contents lists available at ScienceDirect

BBA - Molecular Basis of Disease

journal homepage: www.elsevier.com/locate/bbadis

Connexin43 and zonula occludens-1 are targets of Akt in cardiomyocytes that correlate with cardiac contractile dysfunction in Akt deficient hearts

Sangmi Ock[a,1], Wang Soo Lee[b,1], Hyun Min Kim[a], Kyu-Sang Park[c], Young-Kook Kim[d], Hyun Kook[e], Woo Jin Park[f], Tae Jin Lee[g], E.D. Abel[h,*], Jaetaek Kim[a,**]

[a] Division of Endocrinology and Metabolism, Department of Internal Medicine, College of Medicine, Chung-Ang University, Seoul, Republic of Korea
[b] Division of Cardiology, Department of Internal Medicine, College of Medicine, Chung-Ang University, Seoul, Republic of Korea
[c] Department of Physiology, Yonsei University Wonju College of Medicine, Wonjoo, Republic of Korea
[d] Department of Biochemistry, Chonnam National University Medical School, Gwangju, Republic of Korea
[e] Department of Pharmacology, Medical Research Center for Gene Regulation, Chonnam National University Medical School, Gwangju, Republic of Korea
[f] Department of Life Science, Gwangju Institute of Science and Technology, Gwangju, Republic of Korea
[g] Department of Pathology, College of Medicine, Chung-Ang University, Seoul, Republic of Korea
[h] Fraternal Order of Eagles Diabetes Research Center, Division of Endocrinology and Metabolism, University of Iowa Carver College of Medicine, Iowa City, IA, USA

ARTICLE INFO

Keywords:
Akt isoforms
Heart failure
Gap junction

ABSTRACT

While deletion of *Akt1* results in a smaller heart size and *Akt2*$^{-/-}$ mice are mildly insulin resistant, *Akt1*$^{-/-}$/*Akt2*$^{-/-}$ mice exhibit perinatal lethality, indicating a large degree of functional overlap between the isoforms of the serine/threonine kinase Akt. The present study aimed to determine the cooperative contribution of Akt1 and Akt2 on the structure and contractile function of adult hearts. To generate an inducible, cardiomyocyte-restricted Akt2 knockout (KO) model, *Akt2*$^{flox/flox}$ mice were crossed with tamoxifen-inducible MerCreMer transgenic (MCM) mice and germline *Akt1*$^{-/-}$ mice to generate the following genotypes:*Akt1*$^{+/+}$; *Akt2*$^{flox/flox}$ (WT), *Akt2*$^{flox/flox}$; α-MHC-MCM (*iAkt2* KO), *Akt1*$^{-/-}$, and *Akt1*$^{-/-}$; *Akt2*$^{flox/flox}$; α-MHC-MCM mice (*Akt1*$^{-/-}$/*iAkt2* KO). At 28 days after the first tamoxifen injection, *Akt1*$^{-/-}$/*iAkt2* KO mice developed contractile dysfunction paralleling increased atrial and brain natriuretic peptide (ANP and BNP) levels, and repressed mitochondrial gene expression. Neither cardiac fibrosis nor apoptosis were detected in *Akt1*$^{-/-}$/*iAkt2* KO hearts. To explore potential molecular mechanisms for contractile dysfunction, we investigated myocardial microstructure before the onset of heart failure. At 3 days after the first tamoxifen injection, *Akt1*$^{-/-}$/*iAkt2* KO hearts showed decreased expression of connexin43 (Cx43) and connexin-interacting protein zonula occludens-1 (ZO-1). Furthermore, Akt1/2 silencing significantly decreased both Cx43 and ZO-1 expression in cultured neonatal rat cardiomyocytes in concert with reduced beating frequency. Akt1 and Akt2 are required to maintain cardiac contraction. Loss of Akt signaling disrupts gap junction protein, which might precipitate early contractile dysfunction prior to heart failure in the absence of myocardial remodeling, such as hypertrophy, fibrosis, or cell death.

1. Introduction

The serine/threonine kinase Akt has a high level of evolutionary conservation and plays a key role in the regulation of cellular growth and metabolism [1]. There are three distinct Akt isoforms (Akt1, 2, and 3) that are the products of distinct genes, but are highly related, exhibiting > 80% protein identity and sharing the same structural organization [2]. Akt isoforms are activated by insulin and phosphoinositol-3 kinase (PI3K). Class 1A PI3K (PI3Kα) comprises the p110α catalytic subunit that forms functional heterodimers with various p85 subunit isoforms and mediates the activation of Akt isoforms in response to various growth factors and hormones, such as insulin, insulin-like growth factor-1 (IGF-1), and vascular endothelial growth factor (VEGF), which act via tyrosine kinase receptors. All three isoforms are

* Correspondence to: E. D. Abel, Fraternal Order of Eagles Diabetes Research Center, Division of Endocrinology and Metabolism, University of Iowa Carver College of Medicine, Iowa City, IA 52242, USA.
** Correspondence to: J. Kim, Division of Endocrinology and Metabolism, Department of Internal Medicine, College of Medicine, Chung-Ang University, Seoul 156-755, Republic of Korea.
E-mail addresses: DRCAdmin@uiowa.edu (E.D. Abel), jtkim@cau.ac.kr (J. Kim).
[1] These authors contributed equally to this work.

https://doi.org/10.1016/j.bbadis.2018.01.022
Received 20 October 2017; Received in revised form 12 January 2018; Accepted 23 January 2018
Available online 31 January 2018

expressed in the myocardium; however, Akt1 and Akt2 (Akt1/2) comprise 99% of the Akt protein in the heart [3]. Akt signaling plays an important role in the regulation of cardiac growth and metabolism [4].

Global deletion of *Akt1* resulted in a smaller heart size that was proportional to body size, but with preserved cardiac contractile function [5]. Conversely, overexpression of Akt in isolated cardiomyocytes increased insulin-stimulated protein synthesis, and mice with cardiac overexpression of Akt have greater p70S6K activity and show extreme cardiac hypertrophy [6]. Furthermore, physiological cardiac hypertrophy with preserved contractility developed in the short-term and dilated cardiomyopathy developed in the chronic phase following the induction of activated Akt1 in the heart [7]. Despite the relatively high expression level of Akt2 in the heart, *Akt2* knockout (KO) mice exhibited a normal heart size at baseline, as well as a normal response to IGF-1-stimulated cardiomyocyte growth in culture. Insulin-induced glucose uptake was decreased and fatty acid (FA) oxidation increased in *Akt2* KO mouse cardiomyocytes [8]. These observations suggested that distinct physiological functions of cardiac Akt might be revealed only when total Akt levels are below a critical threshold in the heart. Thus, questions remain regarding the integrated roles of Akt isoforms in cardiac structure and function. Double *Akt1/2* KO mice die shortly after birth [9]; therefore, it was necessary to create inducible or conditional *Akt1/2* KO mice to study the roles of these proteins in the heart.

We aimed to test the hypothesis that Akt1/2 isoforms are required to maintain baseline cardiac function and structure using mutant mice in which *Akt2* was conditionally deleted from the hearts of $Akt1^{-/-}$ mice by introducing a floxed *Akt2* allele and inducing recombination in adult hearts by cardiomyocyte-restricted expression of a tamoxifen-inducible Cre recombinase.

2. Materials and methods

2.1. Generation of mutant mice

To assess the integrated function of the dominant cardiac Akt isoforms, Akt1/2, we first generated inducible cardiomyocyte-specific *Akt2* KO mice by crossing *lox*P-flanked *Akt2* mice (provided by Dr. M. Birnbaum) with MerCreMer (MCM) transgenic mice expressing the Cre recombinase under the control of the α-myosin heavy chain promoter (α-MHC). Tamoxifen treatment activates Cre recombinase in a cardiomyocyte-specific manner [10]. These mice were then crossed with *Akt1* null mice [11] to generate *Akt1* nulls on a background of cardiomyocyte-restricted deletion of *Akt2*. The four experimental groups were WT ($Akt1^{+/+}$; $Akt2^{flox/flox}$), i*Akt2* KO ($Akt2^{flox/flox}$; α-MHC-MCM), $Akt1^{-/-}$, and $Akt1^{-/-}$/i*Akt2* KO ($Akt1^{-/-}$; $Akt2^{flox/flox}$; α-MHC-MCM) mice at 10–12 weeks age. Mice were maintained on a mixed C57BL6J/129Sv background. Animals were fed standard chow and autoclaved water, housed in temperature-controlled, pathogen-free facilities, and maintained in 12 h light/12 h dark conditions. All animal studies were conducted in accordance with guidelines approved by the institutional animal care and use committee of the Chung-Ang University. The investigation conforms with the Guide for the Care and Use of Laboratory Animals published by the US National Institutes of Health.

2.2. Tamoxifen administration to mice

Tamoxifen was dissolved in corn oil to at a final concentration of 4 mg/mL. To induce Akt2 deletion, mice were treated with tamoxifen for four consecutive days at a dose of 40 μg/g (body weight) using a 27-gauge needle by intraperitoneal injection. We injected the same amount of tamoxifen to other experimental groups to exclude confounding results from tamoxifen-induced cardiac toxicity [12].

2.3. Echocardiography

Mice were anesthetized in a chamber using 1.5% isoflurane mixed with 100% oxygen and placed on a heating pad at 37 °C. Echocardiography was performed using the Vevo 770 System (VisualSonics Inc., Toronto, Ontario, Canada) with a 30-MHz transducer in the 2-dimensional M-mode [13].

2.4. Histological analysis

Following deep anesthesia with isoflurane, mice were sacrificed by cervical dislocation. Tissue preparation and staining were performed as described previously [14]. For hematoxylin and eosin, or Masson's trichrome staining, mouse hearts were fixed in 4% paraformaldehyde, embedded in paraffin, and sectioned at a thickness of 4 μm. The slides were examined under an Olympus BX51 microscope. For immunostaining, the hearts were fixed in 4% paraformaldehyde and incubated in 15% sucrose solution overnight at 4 °C and then transferred to 30% sucrose at 4 °C until the tissue sank. The tissue was infiltrated in optimum-cutting-temperature compound (OCT)-filled (Tissue Tek) molds for 30 min at room temperature before freezing. The molds were cooled with liquid nitrogen. After the material had frozen, the tissue was wrapped in aluminum foil and stored at −70 °C. Tissues were then cryosectioned at 6 μm thickness using a cryostat (Leica), prefixed in acetone for 30 min at −70 °C, and then dried briefly until the acetone was removed. The OCT was removed with water. Sections were incubated in blocking solution for 1 h at 37 °C, followed by overnight incubation in primary antibodies [1:50 anti-ZO-1 (Santa Cruz Biotechnology, Santa Cruz, CA, USA), 1:100 anti-CD31 and 1:50 anti-Cx43 (BD Biosciences, San Diego, CA, USA)] at 4 °C. After 5 washes in phosphate-buffered saline (PBS) with 0.1% Triton X-100 (PBST) for 15 min each, the sections were incubated in secondary antibodies [Alexa 568-conjugated rabbit anti-goat IgG, Alexa 488-conjugated goat anti-rat IgG, Alexa 488-conjugated goat anti-mouse IgG (Invitrogen Corp., Carlsbad, CA, USA)] for 1 h at room temperature. After washing with 0.1% PBST, the sections were mounted with DAPI (4′,6-diamidino-2-phenylindole). To measure the myocyte cross-sectional area, sections were stained for membranes with fluorescein isothiocyanate (FITC)-conjugated wheat germ agglutinin (WGA) (Invitrogen). Capillary densities were calculated as the average number of positive staining capillaries per 1 mm^2 from five different fields in all mouse groups. The slides were examined using an LSM 510 and 700 meta laser scanning confocal microscope (Carl Zeiss).

2.5. Terminal deoxynucleotidyl transferase–mediated dUTP nick-end labeling (TUNEL) staining

Apoptosis was determined using an In-Situ Cell Death Detection kit (Roche Diagnostics, Mannheim, Germany). TUNEL staining was performed using slides with frozen sections that were incubated at 37 °C for 60 min with the TUNEL reaction mixture, which included 450 μL of enzyme solution and 50 μL of labeling solution. TUNEL-labeling that colocalized with propidium iodide (PI) staining indicated apoptosis-positive nuclei. TUNEL-positive cells were counted in at least 10 randomly chosen high-power (×40) fields for each mouse.

2.6. Transmission electron microscopy (TEM)

Mouse heart tissues were fixed with 2.5% glutaraldehyde at 4 °C for 24 h. These samples were then rinsed with 0.1 M sodium cacodylate buffer and post-fixed with 1% osmium tetroxide in the same buffer for 2 h. After rinsing with 0.1 M cacodylate buffer, they were dehydrated for 15 min periods in increasing concentrations of ethanol (70, 80, 90, 95, and 100% v/v), exchanged through propylene oxide, and embedded in a mixture of epoxy resin. Sections were cut with a diamond knife on an ultramicrotome (ULTRACUT E, Reichert-Jung, Vienna, Austria) and were stained with 1% uranyl acetate for 14 min, followed by a lead-staining reagent for 3 min. The sections were examined using a transmission electron microscope JEM 1200 EX II (JEOL, Tokyo, Japan).

2.7. Western blotting analysis

Western blotting analysis was performed as described previously [13]. Mouse hearts or neonatal rat cardiomyocytes (NRCMs) were lysed with lysis buffer (20 mM Tris-HCl, pH 7.4; 1% Triton X-100; 1 mM EDTA; 30 mM HEPES; 50 mM $Na_4P_2O_7$; 100 mM NaF) containing 1 × Protease Inhibitor Cocktail (Roche Molecular Biochemicals, Indianapolis, IN, USA) and phosphatase inhibitors. Proteins were resolved by SDS-PAGE and electrotransferred onto nitrocellulose membranes (GE Healthcare, Piscataway, NJ, USA). The antibodies against rabbit anti-Akt (#9272), rabbit anti-Akt2 (#2962), rabbit anti-phospho-p70S6K (#9204), rabbit anti-p70S6K (#9202), rabbit anti-phospho-S6 ribosomal protein (#2211), rabbit anti-S6 ribosomal protein (#2217), rabbit anti-phospho-ERK (#9101), rabbit anti-ERK (#9102), rabbit anti-phospho-JNK (#9251), rabbit anti-JNK (#9252), rabbit anti-GAPDH (#2118) (Cell Signaling Technology), goat anti-ZO-1 (sc-8146), mouse anti-Akt1 (sc-5298) (Santa Cruz Biotechnology), mouse anti-Cx43 (BD Biosciences, 610,062) were used. Immunoreactive proteins were detected using SuperSignal West Femto Maximum Sensitivity Substrate (Thermo Fisher Scientific, Fremont, CA, USA). Densitometric quantitation was achieved using Image J software (NIH).

2.8. RNA isolation and quantitative RT-PCR analysis

Total RNA was obtained from mouse hearts or NRCMs using the RNA-STAT 60 reagent (AMS Biotechnology, Abingdon, UK). To quantify transcripts, a CFX 96 instrument (Bio-Rad Laboratories Inc., Hercules, CA, USA) was used. PCRs were performed using SsoFast™ EvaGreen Supermix (Bio-Rad) and the following primers: mouse *Nppa* (5′-ATGGGCTCCTTCTCCATCA-3′ and 5′-CCTGCTTCCTCAGTCTG CTC-3′), mouse *Nppb* (5′-GGATCTCCT GAAGGTGCTGT-3′ and 5′-TTC TTTTGTGAGGCCTTGGT-3′), mouse *Ndufv1* (5′-TGTGAGACCGTGCTA ATGGA-3′ and 5′-CATCTCCCTTCACAAATCGG-3′), mouse *Ndufa9* (5′-ATCCCTTACCCTTTGCCACT-3′ and 5′-CCGTAGCACCTCAATGG ACT-3′), mouse *Uqcrc1* (5′-TGCCAGAGTTTCCAGACCTT-3′ and 5′-CCA AATGAGACACCAAAGCA-3′), mouse *Ppargc1a* (5′-GTAAATCTGCGGG ATGATGG-3′ and 5′-AGCAGGGTCAAAATCGTCTG-3′), mouse *Ppargc1b* (5′-TGAGGTGTTCGGTGAGATTG-3′ and 5′-CCATAGCTCAGGTGGAA GGA-3′), mouse *Tfam* (5′-CAAAAAGACCTCGTTCAGCA-3′ and 5′-CTTC AGCCATCTGCTCTTCC-3′), mouse *Nrf-1* (5′-CTTCAGAACTGCCAACC ACA-3′ and 5′-GCTTCTGCCAGTGATGCTAC-3′), mouse *Esrra* (5′-GGCG GACGGCAGAAGTACAA-3′ and 5′-CAGGTTCAACCACCAGCAGA-3′), mouse *Ppara* (5′-GAGAATCCACGAAGCCTACC-3′ and 5′-AATCGGACC TCTGCCTCTTT-3′), mouse *Acadm* (5′-ACTGACGCCGTGCAGATTTT-3′ and 5′-GCTTAGTTACACGAGGGTGATG-3′), mouse *Acadl* (5′-ATGGCA AAATACTGGGCATC-3′ and 5′-TCTTGCGATCAGCTCTTTCA-3′), mouse *Actb* (5′-ACCAGTTCGCCATGGATGAC-3′ and 5′-TGCCGGAGCCGTT GTC-3′), mouse *Gja1* (5′-ACAAGTCCTTCCCCA TCTCTCA-3′ and 5′-GTGTGGGCACAGACACGAAT-3′), mouse *Tjp1* (5′- GGAGCTACGCT TGCCACACT-3′ and 5′-GGTCAATCAGGACAGAAACACAGT-3′), rat *Actb* (5′- TATCCTGGCCTCACTGTCCA-3′ and 5′-AAGGGTGTAAAACGCAG CTC-3′), rat *Akt1* (5′-CGGTGAACTCTGACCCTTGT-3′ and 5′-GTAACCC AGGGATGCTCAGA-3′), rat *Akt2* (5′- TGGCAGGATGTGGTACAGAA-3′ and 5′-AGGCTGTCATATCGGTCTGG-3′), rat *Gja1* (5′- GTCTGAGAGCC TGAACTCTCATT-3′ and 5′-TGTCTGGGCACCTCTCTTTC-3′), and rat *Tjp1* (5′- CTTGCCACACTGTGACCCTA -3′ and 5′-AAAGTGGTCAATCA GGACAGAA-3′). To assess the specificity of the amplified PCR products, a post-amplification melting curve analysis was performed and relative quantification was calculated using the comparative cycle threshold (Ct) method.

2.9. Cell culture studies

Two to three-day-old Sprague Dawley rats were killed by decapitation and NRCMs were prepared. NRCMs were incubated in Dulbecco's modified Eagle's medium (DMEM/M199 (1:1)) media containing 10% horse serum (HS), 5% fetal bovine serum (FBS), 1% L-glutamine, 1% bromodeoxyuridine (BrdU) and 1% penicillin/streptomycin. For the short interfering RNA (siRNA) studies, cells were transiently transfected with a negative control siRNA or *Akt1/Akt2* siRNA using Lipofectamine 2000 (Invitrogen), without penicillin/streptomycin, for 4–6 h. After removing the transfection reagent, cells were incubated for 48 h in normal conditioned media. For western blotting and quantitative RT-PCR analysis, cells were harvested using lysis buffer. For immunostaining, transfected cells were fixed with 100% MeOH at −20 °C for 20 min, washed with 0.1% PBST, blocked with 5% BSA, and incubated overnight at 4 °C with anti-Cx43 and anti-ZO-1 antibodies. After three washes in 0.1% PBST for 15 min each, the cells were incubated in secondary antibodies for 1 h at room temperature. After washing with PBS, the cells were mounted on glass slides with mounting medium containing DAPI. To analyze NRCM beating frequency (beat/20 s), beating was recorded for 20 s at similar conditioned areas of syncytium. Some irregular contractions and weak or slow contractions were documented. The beating frequency of syncytium with negative control siRNA was measured in 4 wells. The beating frequency of syncytium with *Akt1/Akt2* siRNA was counted in 5 wells [15].

2.10. Statistical analysis

Data are presented as the mean ± SEM. Statistical analysis was performed using either a Student's *t*-test or an ANOVA with Tukey's *post-hoc* test once normality was demonstrated (Shapiro-Wilk test). Non-normally distributed data were analyzed using either a Mann-Whitney *U* test or a Kruskal-Wallis test followed by a Mann-Whitney *U* test (adjusting the α-level by Bonferroni inequality). The Kaplan-Meier method and log-rank test were used to determine the differences for the estimated survival curves. $P < 0.05$ was considered statistically significant. The statistical analyses were performed using SPSS version 18.0 (IBM Corp., Armonk, NY, USA).

3. Results

3.1. $Akt1^{-/-}$/iAkt2 KO mice display smaller hearts and develop contractile dysfunction

We analyzed mouse cardiac phenotype 28 days after the first tamoxifen injection. Western blotting analysis using heart lysates showed that the total amount of Akt protein was ~10%, indicating Akt was almost completely ablated in $Akt1^{-/-}$/*iAkt2* KO hearts by 28 days after the first tamoxifen injection (Fig. 1A, B). As expected, the body weight before sacrifice showed that $Akt1^{-/-}$ and $Akt1^{-/-}$/*iAkt2* KO mice were 10–15% smaller than the WT or *iAkt2* KO mice (Supplementary material online, Fig. S1A). Heart weight and heart weight normalized for body weight showed that the $Akt1^{-/-}$/*iAkt2* KO mice had smaller hearts compared with the WT, *iAkt2* KO, and $Akt1^{-/-}$ mice (Supplementary material online, Fig. S1B and Fig. 1C). However, measurement of the cardiomyocyte cross-sectional area by wheat germ agglutinin (WGA) staining, which is a surrogate measurement of cardiac volume, showed comparable areas suggesting that short axis cardiomyocyte width was not reduced in the smaller $Akt1^{-/-}$/*iAkt2* KO hearts (Fig. 1D, E).

To assess cardiac contractile function, we performed echocardiography. No difference in fractional shortening was detected among the WT and *iAkt2* KO, and $Akt1^{-/-}$ mice (Fig. 2A, B). By contrast, the $Akt1^{-/-}$/*iAkt2* KO mice displayed cardiac dysfunction. Fractional shortening was reduced by 37.4% in the $Akt1^{-/-}$/*iAkt2* KO mice compared with the WT mice (Fig. 2A, B; Supplementary material online, Table S1). In parallel, mRNA levels of heart failure markers, ANP (encoded by *Nppa*) and BNP (encoded by *Nppb*), increased significantly in the $Akt1^{-/-}$/*iAkt2* KO hearts (Fig. 2C). Furthermore, the expression of genes involved in oxidative phosphorylation, mitochondrial

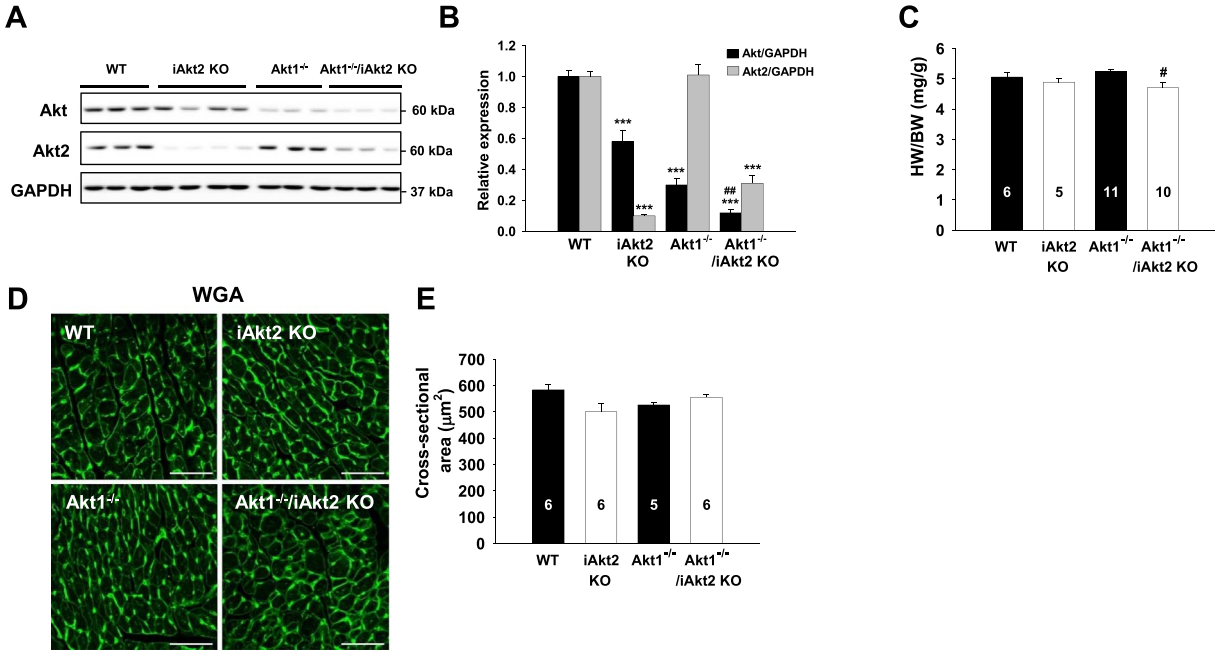

Fig. 1. Heart weight is reduced in *Akt1*$^{-/-}$*/iAkt2* knockout (KO) mice 28 days following the first tamoxifen injection. Representative western blots (A) and densitometric ratios (B) of total Akt and Akt2 proteins from wild-type (WT), *iAkt2* KO, *Akt1*$^{-/-}$, and *Akt1*$^{-/-}$*/iAkt2* KO hearts. Total amount of Akt protein was ~60% in *iAkt2* KO, ~30% in *Akt1*$^{-/-}$, and ~10% in *Akt1*$^{-/-}$*/iAkt2* KO relative to WT hearts. $n = 6$–7 per group. (C) Heart weight to body weight (HW/BW) ratios. Representative immunofluorescence images of heart sections stained with fluorescein isothiocyanate (FITC)-conjugated wheat germ agglutinin (magnification, ×40; scale bars, 30 μm) (D) and quantification of cross-sectional area from at least 100 myocytes per ventricle in randomly selected fields of sections from each genotype (E). Numbers of mice are indicated on the bars. Data are presented as the mean ± SEM. Overall $P < 0.001$ (B) and $P < 0.05$ (C) by one-way ANOVA. ***, $P < 0.001$ versus the WT and #, $P < 0.05$ versus Akt1$^{-/-}$ by Tukey's post-hoc test. ##, $P < 0.01$ versus the WT by Student's *t*-test.

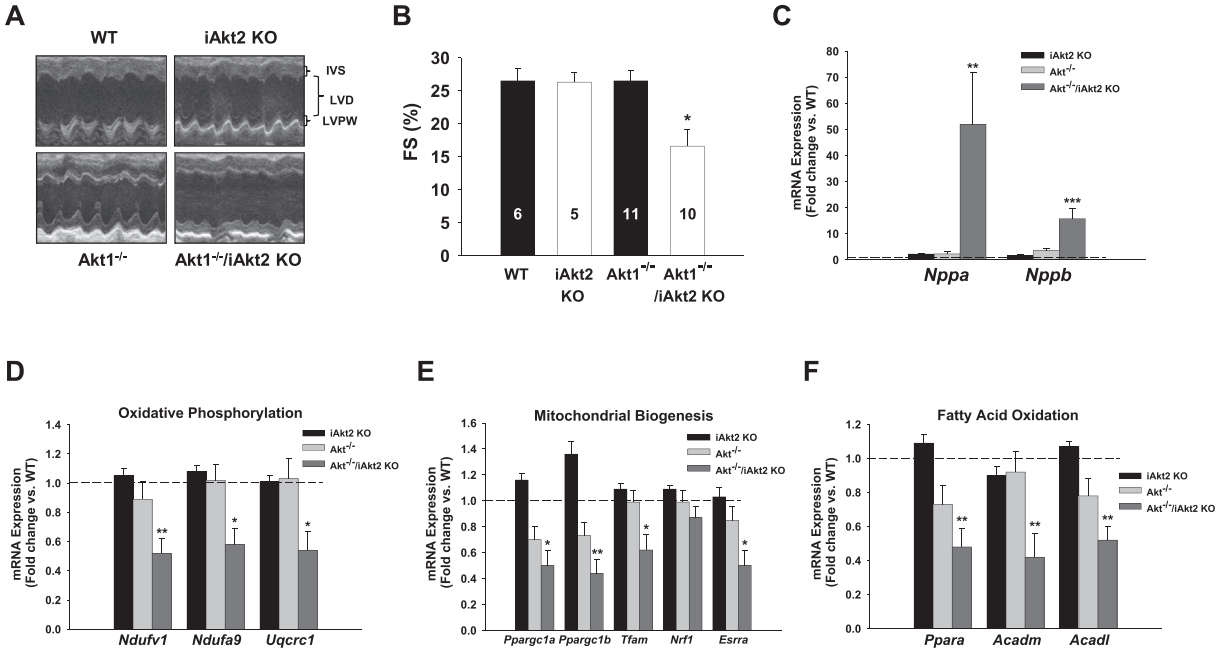

Fig. 2. Cardiac contractile dysfunction and increased heart failure markers in *Akt1*$^{-/-}$*/iAkt2* KO hearts. (A) Representative M-mode echocardiography in all genotypes. (B) Fractional shortening by echocardiography. mRNA quantification of (C) heart failure markers, (D) oxidative phosphorylation, (E) mitochondrial biogenesis, and (F) fatty acid oxidation genes in mice 28 days after the first tamoxifen administration. Results were normalized to the mRNA level of β-actin and mRNA levels in the WT were arbitrarily set as 1. $n = 6$ per group. Data are presented as the mean ± SEM. *, $P < 0.05$; **, $P < 0.01$; ***, $P < 0.001$ versus the WT.

biogenesis, and fatty acid oxidation were repressed in the *Akt1*$^{-/-}$*/iAkt2* KO hearts (Fig. 2D–F).

3.2. *Akt1*$^{-/-}$*/iAkt2 KO mice display normal myocardial structural remodeling*

To further evaluate the structural remodeling in failing *Akt1*$^{-/-}$*/iAkt2* KO hearts, we analyzed cardiac histology. H&E staining showed normal gross cardiac morphology in all genotypes (Fig. 3A). Capillary densities were preserved and interstitial fibrosis was not increased in *Akt1*$^{-/-}$*/iAkt2* KO hearts (Fig. 3B–E). Furthermore, no cardiomyocyte apoptosis was found in any genotype (Fig. 3F, G). Surprisingly, mortality at 28 days did not differ between the WT and *Akt1*$^{-/-}$*/iAkt2* KO mice, indicating mild cardiac dysfunction

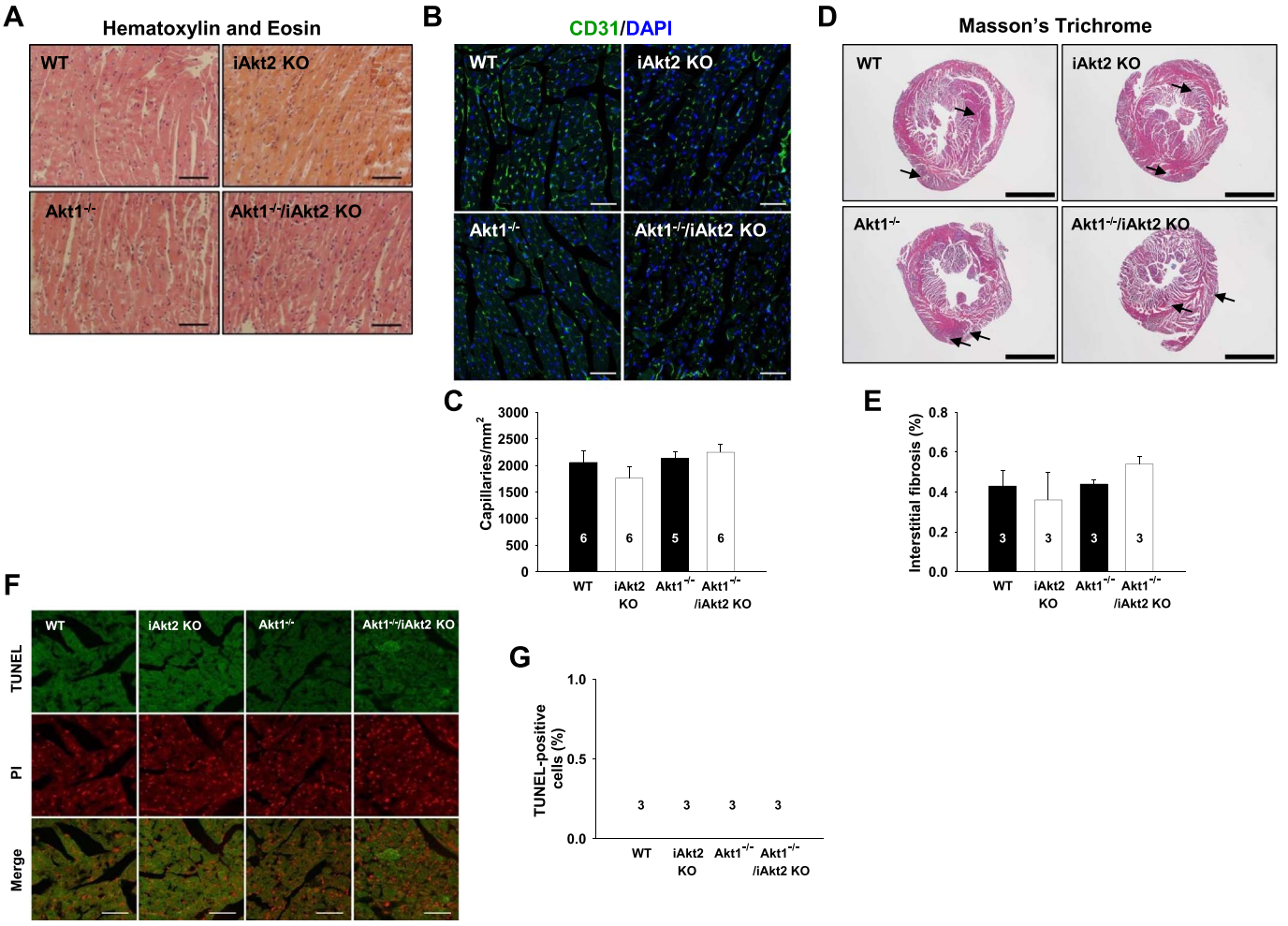

Fig. 3. Preserved cardiac architecture in *Akt1*$^{-/-}$*/iAkt2* KO hearts. (A) Representative hematoxylin and eosin staining (magnification, ×40; scale bars, 30 μm). (B) Representative CD31 staining (magnification, ×20; scale bars, 50 μm) and (C) quantification of capillary density. (D) Representative Masson's trichrome staining (Arrows indicate positive staining, magnification, ×2; scale bars, 2 mm) and (E) quantification of interstitial fibrosis. (F) Representative Terminal deoxynucleotidyl transferase–mediated dUTP nick-end labeling (TUNEL) staining (magnification, ×40; scale bars, 30 μm) and (G) quantification of apoptotic cells. Numbers of mice are indicated on the bars.

(Supplementary material online, Fig. S2).

3.3. Downregulation of gap junction proteins precede contractile dysfunction in the *Akt1*$^{-/-}$*/iAkt2* KO mice

To understand the potential mechanisms that induce contractile dysfunction in the *Akt1*$^{-/-}$*/iAkt2* KO mice, we examined the hearts before the functional changes occurred. Serial echocardiography was performed in all genotypes at 3 and 4 days after the first tamoxifen injection. Fractional shortening decreased significantly in the *Akt1*$^{-/-}$*/iAkt2* KO mice from 4 days (Supplementary material online, Table S2). Thus, we examined mouse hearts at 3 days after the first tamoxifen injection. Western blotting analysis showed that two consecutive tamoxifen injections effectively reduced Akt2 expression in *iAkt2* KO and *Akt1*$^{-/-}$*/iAkt2* KO hearts (Fig. 4B, C). Phosphorylation of p70S6K and S6 ribosomal protein increased in *iAkt2* KO and *Akt1*$^{-/-}$*/iAkt2* KO hearts, suggesting that *Akt2* deletion caused compensatory activation of p70S6K signaling. We also observed an increase in Erk phosphorylation in *Akt1*$^{-/-}$ and *Akt1*$^{-/-}$*/iAkt2* KO hearts. Notably, phosphorylation of JNK was increased in only *Akt1*$^{-/-}$*/iAkt2* KO hearts, which appears to be attributable to deletion of both *Akt1* and *Akt2* in the heart. It has been shown that JNK activation mediates downregulation of gap junction protein connexin (Cx)43 in cardiomyocytes [16]. Furthermore, zonula occludens (ZO)-1 was found to be colocalized with Cx43 at intercalated disks, and diminished ZO-1 expression coincides with reduced Cx43 staining in failing hearts [17]. Thus, we investigated whether enhanced JNK phosphorylation is associated with the downregulation of Cx43 and ZO-1 in the *Akt1*$^{-/-}$*/iAkt2* KO hearts. As shown in Fig. 4A, mRNA expression of Cx 43, but not ZO-1, was reduced in *Akt1*$^{-/-}$*/iAkt2* KO compared to WT hearts, indicating only Cx43 is transcriptionally regulated by Akt1/2. Western blotting showed that Cx43 and ZO-1 protein levels were decreased in the *Akt1*$^{-/-}$*/iAkt2* KO hearts (Fig. 4B, C). Double immunofluorescence showed that Cx43/ZO-1 were stained linearly and colocalized in WT hearts. In contrast, diminished signal was detected in the *Akt1*$^{-/-}$*/iAkt2* KO hearts (Fig. 4D, E). In addition, electron microscopy further verified the disrupted gap junction integrity in the Akt1$^{-/-}$/iAkt2 KO hearts (Fig. 4F). Thus, it is plausible that an imbalance of Akt versus Erk/JNK signaling could contribute to the detrimental outcomes, which may be initiated by the Cx43/ZO-1 disruption.

3.4. Deficiency of Akt1/2 depresses the expression of Cx43 and ZO-1 and beat frequency in cardiomyocytes

To further investigate the functional effect of Akt1/2 deletion on Cx43 and ZO-1 expression and cardiomyocyte contraction, we studied neonatal rat cardiomyocytes (NRCMs) as an in vitro model system because these cells typically show spontaneous beating after plating [18]. We assessed whether *Akt1/2* deficiency suppressed Cx43/ZO-1 and NRCM contraction. We treated NRCMs with control or *Akt1/2* siRNAs.

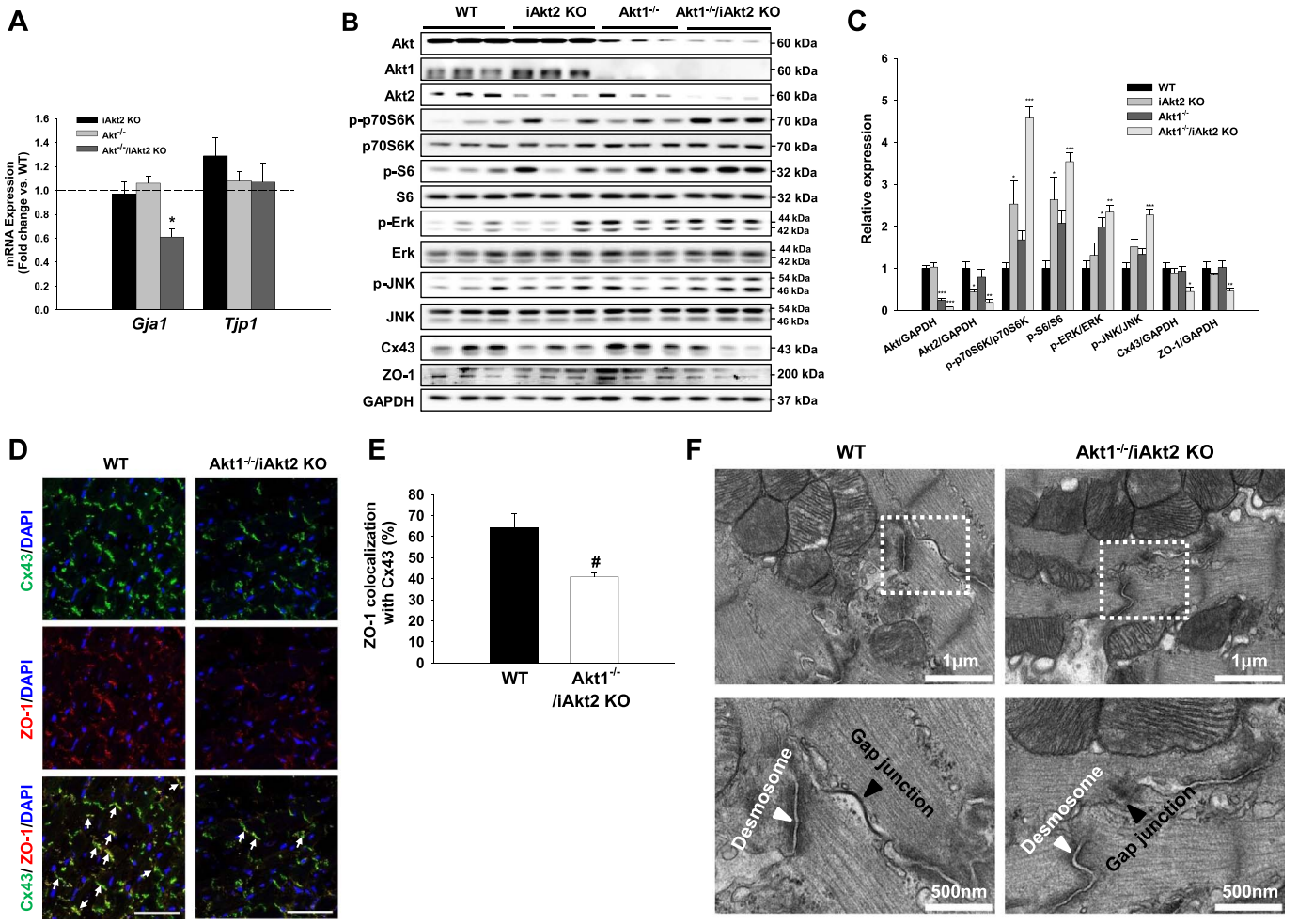

Fig. 4. *Akt1/2* deletion decreases myocardial Cx43 and ZO-1 protein. (A) mRNA quantification of Cx43 (encoded by *Gja1*) and ZO-1 (encoded by *Tjp1*) from WT, *iAkt2* KO, *Akt1*$^{-/-}$, and *Akt1*$^{-/-}$*/iAkt2* KO hearts at 3 days after the first tamoxifen administration. Results were normalized to the mRNA level of β-actin and mRNA levels in the WT and were arbitrarily set as 1. n = 7–10 per group. Western blotting analysis (B) and densitometric ratios (C) from WT, *iAkt2* KO, *Akt1*$^{-/-}$, and *Akt1*$^{-/-}$*/iAkt2* KO hearts. n = 5–8 per group. (D) Representative immunostaining for Cx43 (green) or ZO-1 (red) is shown overlaid with 4′,6-diamidino-2-phenylindole (DAPI)-stained nuclei (blue). Arrows indicate Cx43/ZO-1 colocalization (magnification, ×40; scale bars, 50 μm). (E) Quantification of colocalization of Cx43 and ZO-1 was performed using ImageJ. n = 3 per group. (F) Representative longitudinal electron microscopy images of the intercalated disks of left ventricular wall [magnification, ×30 K (*upper panel*), ×60 K (*lower panel*)]. The WT heart shows a gap junction in close proximity to desmosome (*left panel*). In contrast, Akt1$^{-/-}$/iAkt2 KO hearts shows a faint gap junction with a preserved desmosome (*right panel*). Data are presented as the mean ± SEM. $^{\#}$, $P < 0.05$ versus WT. Overall $P < 0.01$ (quantitative RT-PCR for Cx43, western blotting for Akt2, p-Erk, Cx43, ZO-1), and $P < 0.001$ (Akt, p-p70S6K, p-S6, p-JNK) by one-way ANOVA. *, $P < 0.05$; **, $P < 0.01$; ***, $P < 0.001$ versus the WT by Tukey's post-hoc test or Mann-Whitney U test.

Knockdown of *Akt1/2* reduced Cx43 and ZO-1 mRNA expression and colocalization and distribution in the cell membrane (Fig. 5A, B) indicating Cx43 and ZO-1 are transcriptionally regulated in cardiomyocyte. Western blotting analysis also showed downregulation of Cx43 and ZO-1 protein levels in *Akt1/2* siRNA-treated NRCMs (Fig. 5C). Furthermore, the beating frequency decreased significantly in *Akt1/2* knockdown cells (Fig. 5D, E). These data suggest that reduced Cx43 and ZO-1 might contribute to cardiac dysfunction in *Akt1*$^{-/-}$*/iAkt2* KO hearts.

4. Discussion

The present study demonstrated that cardiac-specific *Akt1*$^{-/-}$*/iAkt2* KO in mice reduces cardiac size and induces contractile dysfunction without myocardial structural remodeling, such as interstitial fibrosis, hypertrophy, and apoptosis. Moreover, *Akt1*$^{-/-}$*/iAkt2* KO hearts showed decreased expression of Cx43 and connexin-interacting protein ZO-1. These studies identify a previously unrecognized mechanism by which Akt isoforms maintain cardiac contractile function, namely gap junction protein stability.

Targeted disruption of the *Akt1* gene in mice induces a growth retardation phenotype [4,19]. *Akt2* KO mice reveal mild growth retardation and insulin resistance [4,20,21]. *Akt1/2* double KO (DKO) mice display severe growth deficiency and die shortly after birth. These mice exhibit impaired bone and skin development and severe skeletal muscle atrophy because of a marked decrease in individual muscle cell size, and impeded adipogenesis [9]. However, the effect of cardiac-specific *Akt1/2* DKO on cardiac function and structure remains to be systematically investigated. The present study revealed an association between cardiac dysfunction and expression of gap junction proteins, Cx43 and ZO-1, which are regulated by Akt1/2.

In vertebrates, gap junctions are present in most tissues and play important roles in growth regulation, development, cell-to-cell communication, and tissue homeostasis [22]. They are organized from hexameric connexin hemichannels, encoded by 21 or 20 distinct genes in humans or rodents respectively [23]. The major cardiac connexin proteins are Cx40, Cx43, and Cx45, having obvious expression patterns and essential roles in heart development, metabolic coupling, propagation of action potentials, and tissue homeostasis [24–29]. The tight junction protein ZO-1 is a member of the membrane-associated guanylate kinase (MAGUK) family of proteins [30]. A previous study showed that ZO-1 was found at 96% of the intercalated discs in non-

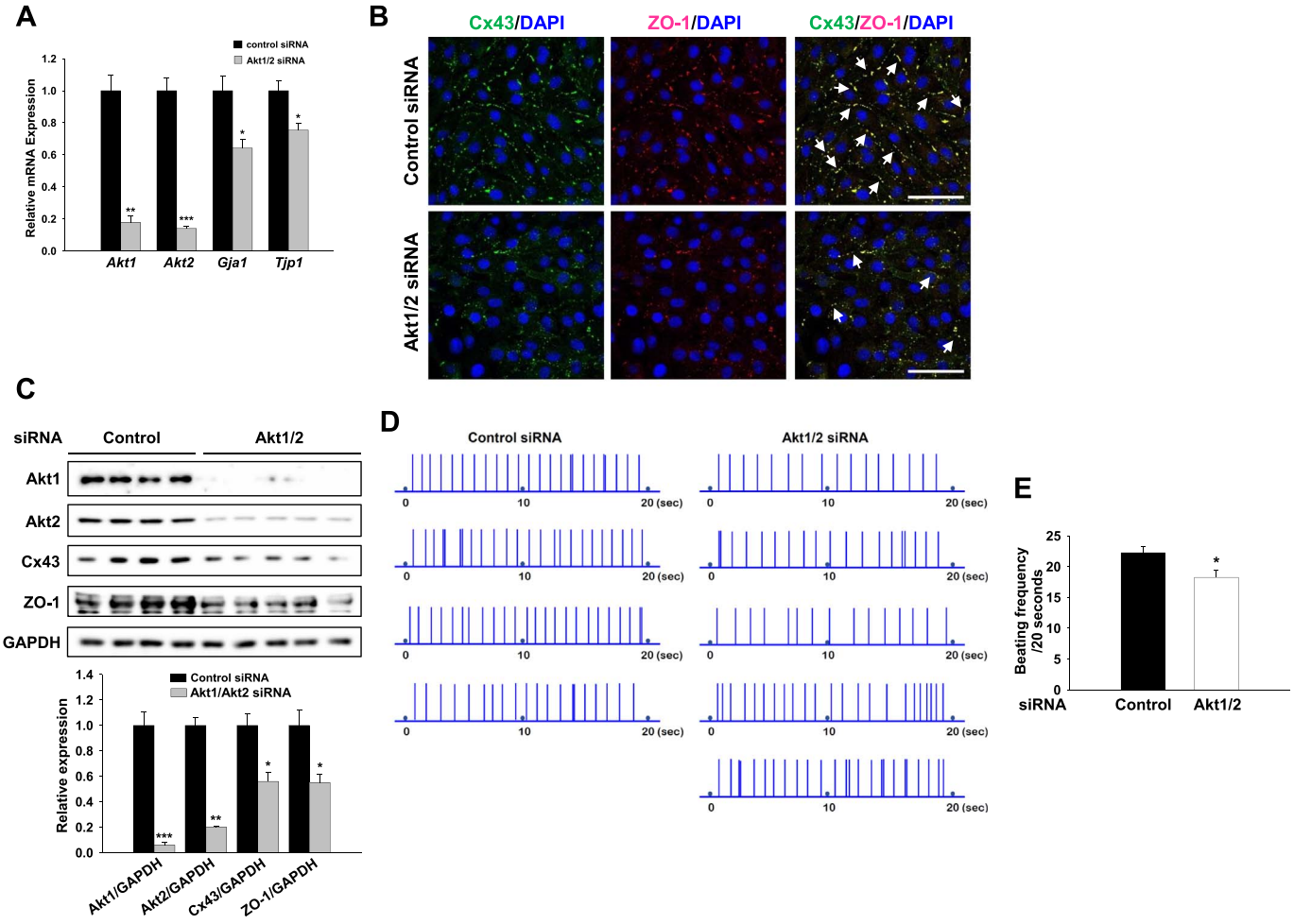

Fig. 5. *Akt1/2* knockdown reduces Cx43 and ZO-1 expression in cultured neonatal rat cardiomyocytes (NRCMs).
(A) mRNA quantification of *Akt1*, *Akt2*, *Gja1*, and *Tjp1* from control or Akt1/2 siRNA treated cells. Results were normalized to the mRNA level of β-actin and mRNA levels in the control cells and were arbitrarily set as 1. $n = 5$ per group. (B) Representative immunostaining for Cx43 (green), ZO-1 (red), and merged image overlaid with 4′,6-diamidino-2-phenylindole (DAPI)-stained nuclei (blue). Arrows indicate Cx43/ZO-1 colocalization (magnification, ×40; scale bars, 50 μm). (C) Western blot analysis (*upper panel*) and densitometric ratios (*lower panel*) of Akt1, Akt2, Cx43, and ZO-1 after treatment with control short interfering RNA (siRNA) or *Akt1/2* siRNA for 48 h. n = 5–8. DAPI was used to detect nuclei. NRCM beating frequency was recorded (D) and quantified (E). Four independent experiments were performed. *, $P < 0.05$; **, $P < 0.01$; ***, $P < 0.001$ versus the control siRNA. (For interpretation of the references to color in this figure legend, the reader is referred to the web version of this article.)

failing human hearts, where it colocalized with Cx43. In contrast, ZO-1 immunostaining was observed in only 5% of intercalated discs in failing hearts, coincident with a reduction in Cx43 staining. Immunoblotting analysis showed that there was a 95% reduction in ZO-1 expression in human heart failure. Loss of ZO-1 at intercalated discs in heart failure might play a critical role in remodeling Cx43 gap junctions [30]. Divergent interactions between connexins and the tight junction proteins ZO-1, ZO-2, and ZO-3 in regulating connexins in gap junction transition have been described and vary depending on the connexin protein [31–34]. Increased interaction between ZO-1 and Cx43 has been implicated in Cx43 downregulation and reduced Cx43 gap junction size in congestive heart failure [35]. The novel finding of the present study is that *Akt1*$^{-/-}$*/iAkt2* KO mice demonstrate abnormal gap junction structure and downregulation of Cx43 and ZO-1, prior to the onset of contractile dysfunction, which was evident as early as three days after the first tamoxifen injection. These results suggested that the Akt pathway is important to conserve gap junction proteins, which might play an important role in maintaining cardiac contractility.

Another interesting finding of the present study was the early onset of heart failure in the absence of structural remodeling developing as early as four days after the first tamoxifen injection. In another study using a cardiac-specific KO mice model, *IRS1/2* DKO mice exhibited heart failure with cell death, fibrosis, and decreased ventricular mass at the age of 5 weeks [36]. In contrast, the present study using the *Akt1*$^{-/-}$*/iAkt2* KO model induced heart failure at the age of 4 days. These two different DKO models support the view that insulin signaling defects can induce heart failure, despite clear differences in the timing and characteristics of heart failure. *Akt1*$^{-/-}$*/iAkt2* KO mice developed heart failure at 4 days after the loss of *Akt1/2*, with a very rapid onset, without typical characteristics of heart failure, such as cell death and fibrosis. These results imply that distinct mechanisms induce the early-onset heart failure in *Akt1*$^{-/-}$*/iAkt2* KO mice in the absence of gross pathological changes that characterize other models with long-term reduction of upstream activators of Akt such as IRS proteins [37]. Taken together, we speculate that reduction of Cx43 and ZO-1 expression by reduced Akt1 and Akt2 signaling represents an early defect that may contribute to cardiac dysfunction.

There are some limitations and further experiments that are required. First, to our surprise, measurement of the cardiomyocyte cross-sectional area in *Akt1*$^{-/-}$*/iAkt2* KO mice showed comparable areas to WT mouse despite of reduced heart weight. In addition to measuring cardiomyocyte cross-sectional area, measurement of long and short axis cell width of H&*E*-stained cardiomyocytes in the left ventricle would be useful to assess cardiomyocyte volume in the smaller *Akt1*$^{-/-}$*/iAkt2* KO hearts. Second, in the strict sense, the present study is not a cardiomyocyte-specific DKO mouse model because the *Akt2* gene is deleted

specifically in cardiomyocytes, but not the *Akt1* gene. The *Akt1* gene was removed in all cardiac tissues, including fibroblasts and cardiomyocytes. Moreover, because Akt1 deficiency occurred in the germline, it is possible that long-term adaptations to Akt1 deficiency could confound the cardiac response to inducible deletion of Akt2 in Akt1 null cardiomyocytes. Therefore, it will be necessary to compare the phenotype of cardiomyocyte-specific *Akt1/2* DKO mice with that of *Akt1*$^{-/-}$*/iAkt2* KO mice described in this study. Thus, it is possible that inducible cardiomyocyte-specific *Akt1/2* DKO mice could exhibit more striking phenotypes. Third, this study has not explored other potential mechanisms leading to cardiac dysfunction in *Akt1*$^{-/-}$*/iAkt2* KO mice such as potential changes in cytoskeletal proteins. Previous studies proposed that ZO-1 interacts with other cytoskeleton proteins in addition to Cx43 [38–40]. Barker et al. showed that ZO-1 stabilizes the gap junction through anchoring of actin filaments, an important major cytoskeleton protein associated with contractile function [38]. Another study revealed that permeability of Cx43-containing channels was regulated dynamically by F-actin and the small G-protein RhoA, which are major regulators of cellular junctions and the actin cytoskeleton [39]. In addition, although not a study using cardiomyocytes, it was reported that disruption of the Cx43/ZO-1 complex induced collapse of the organized F-actin cytoskeleton [40]. Therefore, future studies will further explore the contributions of changes in other cytoskeleton proteins in the *Akt1*$^{-/-}$*/iAkt2* KO mouse model that might contribute to the acute heart failure that develops in the absence of gross pathological changes as early as 4 days after deletion of *Akt1* and *Akt2*.

In conclusion, Akt isoforms are required to maintain cardiac contractile function that correlates with maintenance of gap junctions by Cx43 and ZO-1, prior to the development of gross myocardial remodeling, characterized by myocyte hypertrophy, fibrosis, or cell death.

Supplementary data to this article can be found online at https://doi.org/10.1016/j.bbadis.2018.01.022.

Transparency document

The http://dx.doi.org/10.1016/j.bbadis.2018.01.022 associated with this article can be found in online version.

Disclosure statement

The authors declare that they have no conflicts of interest with the contents of this article.

Funding

This work was supported by grants of the Basic Science Research Program through the National Research Foundation of Korea (NRF) funded by the Ministry of Science, ICT & Future Planning [2009-0077202 to JK, 2016R1A4A1009895 to YKK, HK, WJP, JK] and by grant U01 HL087947 from the National Institutes of Health to EDA.

References

[1] M.P. Scheid, J.R. Woodgett, PKB/AKT: functional insights from genetic models, Nat. Rev. Mol. Cell Biol. 2 (2001) 760–768.
[2] A. Bellacosa, J.R. Testa, R. Moore, L. Larue, A portrait of AKT kinases: human cancer and animal models depict a family with strong individualities, Cancer Biol. Ther. 3 (2004) 268–275.
[3] T. Matsui, A. Rosenzweig, Convergent signal transduction pathways controlling cardiomyocyte survival and function: the role of PI 3-kinase and Akt, J. Mol. Cell. Cardiol. 38 (2005) 63–71.
[4] I. Shiojima, K. Walsh, Regulation of cardiac growth and coronary angiogenesis by the Akt/PKB signaling pathway, Genes Dev. 20 (2006) 3347–3365.
[5] B. DeBosch, I. Treskov, T.S. Lupu, C. Weinheimer, A. Kovacs, M. Courtois, A.J. Muslin, Akt1 is required for physiological cardiac growth, Circulation 113 (2006) 2097–2104.
[6] T. Matsui, L. Li, J.C. Wu, S.A. Cook, T. Nagoshi, M.H. Picard, R. Liao, A. Rosenzweig, Phenotypic spectrum caused by transgenic overexpression of activated Akt in the heart, J. Biol. Chem. 277 (2002) 22896–22901.
[7] I. Shiojima, K. Sato, Y. Izumiya, S. Schiekofer, M. Ito, R. Liao, W.S. Colucci, K. Walsh, Disruption of coordinated cardiac hypertrophy and angiogenesis contributes to the transition to heart failure, J. Clin. Invest. 115 (2005) 2108–2118.
[8] B. DeBosch, N. Sambandam, C. Weinheimer, M. Courtois, A.J. Muslin, Akt2 regulates cardiac metabolism and cardiomyocyte survival, J. Biol. Chem. 281 (2006) 32841–32851.
[9] X.D. Peng, P.Z. Xu, M.L. Chen, A. Hahn-Windgassen, J. Skeen, J. Jacobs, D. Sundararajan, W.S. Chen, S.E. Crawford, K.G. Coleman, N. Hay, Dwarfism, impaired skin development, skeletal muscle atrophy, delayed bone development, and impeded adipogenesis in mice lacking Akt1 and Akt2, Genes Dev. 17 (2003) 1352–1365.
[10] D.S. Sohal, M. Nghiem, M.A. Crackower, S.A. Witt, T.R. Kimball, K.M. Tymitz, J.M. Penninger, J.D. Molkentin, Temporally regulated and tissue-specific gene manipulations in the adult and embryonic heart using a tamoxifen-inducible Cre protein, Circ. Res. 89 (2001) 20–25.
[11] H. Cho, J.L. Thorvaldsen, Q. Chu, F. Feng, M.J. Birnbaum, Akt1/PKBalpha is required for normal growth but dispensable for maintenance of glucose homeostasis in mice, J. Biol. Chem. 276 (2001) 38349–38352.
[12] K. Bersell, S. Choudhury, M. Mollova, B.D. Polizzotti, B. Ganapathy, S. Walsh, B. Wadugu, S. Arab, B. Kühn, Moderate and high amounts of tamoxifen in alphaMHC-MerCreMer mice induce a DNA damage response, leading to heart failure and death, Dis. Model. Mech. 6 (2013) 1459–1469.
[13] S. Ock, J. Ahn, S.H. Lee, H. Park, J.W. Son, J.G. Oh, D.K. Yang, W.S. Lee, H.S. Kim, J. Rho, G.T. Oh, E.D. Abel, W.J. Park, J.K. Min, J. Kim, Receptor activator of nuclear factor-kappaB ligand is a novel inducer of myocardial inflammation, Cardiovasc. Res. 94 (2012) 105–114.
[14] S. Ock, W.S. Lee, J. Ahn, H.M. Kim, H. Kang, H.S. Kim, D. Jo, E.D. Abel, T.J. Lee, J. Kim, Deletion of IGF-1 receptors in cardiomyocytes attenuates cardiac aging in male mice, Endocrinology 157 (2016) 336–345.
[15] C.K. Liao, H.H. Cheng, S.D. Wang, D.F. Yeih, S.M. Wang, PKCε mediates serine phosphorylation of connexin43 induced by lysophosphatidylcholine in neonatal rat cardiomyocytes, Toxicology 314 (2013) 11–21.
[16] B.G. Petrich, X. Gong, D.L. Lerner, X. Wang, J.H. Brown, J.E. Saffitz, Y. Wang, c-Jun N-terminal kinase activation mediates downregulation of connexin43 in cardiomyocytes, Circ. Res. 91 (2002) 640–647.
[17] S. Kostin, Zonula occludens-1 and connexin 43 expression in the failing human heart, J. Cell. Mol. Med. 11 (2007) 892–895.
[18] E. Ehler, T. Moore-Morris, S. Lange, Isolation and culture of neonatal mouse cardiomyocytes, J. Vis. Exp. 79 (2013) e50154.
[19] W.S. Chen, P.Z. Xu, K. Gottlob, M.L. Chen, K. Sokol, T. Shiyanova, I. Roninson, W. Weng, R. Suzuki, K. Tobe, T. Kadowaki, N. Hay, Growth retardation and increased apoptosis in mice with homozygous disruption of the Akt1 gene, Genes Dev. 15 (2001) 2203–2208.
[20] H. Cho, J. Mu, J.K. Kim, J.L. Thorvaldsen, Q. Chu, E.B. Crenshaw 3rd, K.H. Kaestner, M.S. Bartolomei, G.I. Shulman, M.J. Birnbaum, Insulin resistance and a diabetes mellitus-like syndrome in mice lacking the protein kinase Akt2 (PKB beta), Science 292 (2001) 1728–1731.
[21] R.S. Garofalo, S.J. Orena, K. Rafidi, A.J. Torchia, J.L. Stock, A.L. Hildebrandt, T. Coskran, S.C. Black, D.J. Brees, J.R. Wicks, J.D. McNeish, K.G. Coleman, Severe diabetes, age-dependent loss of adipose tissue, and mild growth deficiency in mice lacking Akt2/PKB beta, J. Clin. Invest. 112 (2003) 197–208.
[22] S. Kurtenbach, S. Kurtenbach, G. Zoidl, Gap junction modulation and its implications for heart function, Front. Physiol. 5 (2014) 82.
[23] G. Sohl, S. Maxeiner, K. Willecke, Expression and functions of neuronal gap junctions, Nat. Rev. Neurosci. 6 (3) (2005) 191–200.
[24] C.W. Lo, Role of gap junctions in cardiac conduction and development: insights from the connexin knockout mice, Circ. Res. 87 (2000) 346–348.
[25] K. Nishii, M. Kumai, Y. Shibata, Regulation of the epithelial-mesenchymal transformation through gap junction channels in heart development, Trends Cardiovasc. Med. 11 (2001) 213–218.
[26] S. Rohr, Role of gap junctions in the propagation of the cardiac action potential, Cardiovasc. Res. 62 (2004) 309–322.
[27] S.A. Bernstein, G.E. Morley, Gap junctions and propagation of the cardiac action potential, Adv. Cardiol. 42 (2006) 71–85.
[28] S. Zacchigna, H. Oh, M. Wilsch-Brauninger, E. Missol-Kolka, J. Jaszai, S. Jansen, N. Tanimoto, F. Tonagel, M. Seeliger, W.B. Huttner, D. Corbeil, M. Dewerchin, S. Vinckier, L. Moons, P. Carmeliet, Loss of the cholesterol-binding protein prominin-1/CD133 causes disk dysmorphogenesis and photoreceptor degeneration, J. Neurosci. 29 (2009) 2297–2308.
[29] J.A. Jansen, T.A. van Veen, J.M. de Bakker, H.V. van Rijen, Cardiac connexins and impulse propagation, J. Mol. Cell. Cardiol. 48 (2010) 76–82.
[30] J.G. Laing, J.E. Saffitz, T.H. Steinberg, K.A. Yamada, Diminished zonula occludens-1 expression in the failing human heart, Cardiovasc. Pathol. 16 (2007) 159–164.
[31] B.N. Giepmans, W.H. Moolenaar, The gap junction protein connexin43 interacts with the second PDZ domain of the zona occludens-1 protein, Curr. Biol. 8 (1998) 931–934.
[32] T. Toyofuku, M. Yabuki, K. Otsu, T. Kuzuya, M. Hori, M. Tada, Direct association of the gap junction protein connexin-43 with ZO-1 in cardiac myocytes, J. Biol. Chem. 273 (1998) 12725–12731.
[33] P.J. Kausalya, M. Reichert, W. Hunziker, Connexin45 directly binds to ZO-1 and localizes to the tight junction region in epithelial MDCK cells, FEBS Lett. 505 (2001) 92–96.
[34] J.M. Rhett, J. Jourdan, R.G. Gourdie, Connexin 43 connexon to gap junction transition is regulated by zonula occludens-1, Mol. Biol. Cell 22 (2011) 1516–1528.
[35] A.F. Bruce, S. Rothery, E. Dupont, N.J. Severs, Gap junction remodelling in human

heart failure is associated with increased interaction of connexin43 with ZO-1, Cardiovasc. Res. 77 (2008) 757–765.
[36] Y. Qi, Z. Xu, Q. Zhu, C. Thomas, R. Kumar, H. Feng, D.E. Dostal, M.F. White, K.M. Baker, S. Guo, Myocardial loss of IRS1 and IRS2 causes heart failure and is controlled by p38alpha MAPK during insulin resistance, Diabetes 62 (2013) 3887–3900.
[37] C. Riehle, A.R. Wende, S. Sena, K.M. Pires, R.O. Pereira, Y. Zhu, H. Bugger, D. Frank, J. Bevins, D. Chen, C.N. Perry, X.C. Dong, S. Valdez, M. Rech, X. Sheng, B.C. Weimer, R.A. Gottlieb, M.F. White, E.D. Abel, Insulin receptor substrate signaling suppresses neonatal autophagy in the heart, J. Clin. Invest. 123 (2013) 5319–5333.
[38] R.J. Barker, R.L. Price, R.G. Gourdie, Increased association of ZO-1 with connexin43 during remodeling of cardiac gap junctions, Circ. Res. 90 (2002) 317–324.
[39] M. Derangeon, N. Bourmeyster, I. Plaisance, C. Pinet-Charvet, Q. Chen, F. Duthe, M.R. Popoff, D. Sarrouilhe, J.C. Hervé, RhoA GTPase and F-actin dynamically regulate the permeability of Cx43-made channels in rat cardiac myocytes, J. Biol. Chem. 283 (2008) 30754–30765.
[40] C.H. Chen, J.N. Mayo, R.G. Gourdie, S.R. Johnstone, B.E. Isakson, S.E. Bearden, The connexin 43/ZO-1 complex regulates cerebral endothelial F-actin architecture and migration, Am. J. Phys. Cell Phys. 309 (2015) C600–607.